The impact of wind direction in atmospheric BL on interacting wakes at Horns Rev wind farm

Ivanell, Stefan; Mikkelsen, Robert Flemming; Sørensen, Jens Nørkær; Hansen, Kurt Schaldemose; Henningson, Dan

Published in:
Torque 2010

Publication date:
2010

The impact of wind direction in atmospheric BL on interacting wakes at Horns Rev wind farm

S Ivanell[1,2], R Mikkelsen[3], J N Sørensen[3], K S Hansen[3], D Henningson[1]

[1]Linné Flow Centre, Department of Mechanics, KTH, Stockholm, Sweden

[2]Gotland University, Visby, Sweden

[3]Department of Mechanical Engineering, DTU, Lyngby, Denmark

Abstract

Large eddy simulations of the Navier-Stokes equations are performed to simulate the Horns Rev off shore wind farm 15 km outside the Danish west coast. The aim is to achieve a better understanding of the wake interaction inside the farm. The simulations are performed by combining the in-house developed computer code EllipSys3D with the actuator-disc methodology. In the actuator-disc method the blades are represented by a disc at which body forces representing the aerodynamic loading are introduced. The body forces are determined by computing local angles of attack and tabulated aerofoil coefficients. The advantage of using the actuator-disc technique is that it is not necessary to resolve blade boundary layers since the computational resources are devoted to simulating the dynamics of the flow structures.

In the present study approximately 13.6 million mesh points are used to resolve the wake structure in the park.

The results from the CFD simulations are evaluated and the downstream evolution of the velocity field is depicted. Special interest is given to what extent the production is dependent on the inflow angle and turbulence level.

The study shows that the applied method captures the main production variation within the wind farm. The result further demonstrates that levels of production correlate well with measurements. However, in some cases the variation of the measurement data is caused by variation of measurement conditions with inflow angles.

The study also shows that the wind veer has a significant impact on the wake interaction and power losses of downstream turbine positions.

1 Introduction

Today, the trend is to build wind turbines in large clusters, both on-shore and off-shore. In both cases this means that the turbines operate in the wakes of each other and, depending on the wind direction, they can be subject to inflow conditions dominated by vortical structures created by upstream turbines. This reduces the power performance for the individual wind turbine as well as decreasing the life time of the rotors. Hence, there is a need for understanding and modelling the wake behaviour of wind turbines.

Wakes behind wind turbines can be distinctly divided into near and far wake regions. The study of near wake aerodynamics concerns the description of the vortices in the wake and their relationship to the blade loading and inflow conditions. The near wake is followed by the far wake where the focus is put on the influence of wind turbines in a farm situation where the modelling of the actual rotor is less important. In the far wake, turbulence, wake interaction and topographic effects are of primary interest.

The present work deals with numerical simulation of a cluster of up to 20 turbines. Earlier studies by Ivanell et al., [7], [6], using actuator line techniques have been performed to study the details of the near wake of a single turbine. Whereas the actuator line method is computationally expensive, the use of actuator discs may capture the main aerodynamic effects of power, thrust and deficit at a much reduced computational cost. Thus the actuator discs are used with poorer but satisfactory resolution in order to capture the flow through and between the turbines.

Earlier work in this area has been performed e.g. by Ammara et al., [1] and by Mikkelsen, Troldborg et al., [16], [25]. Ammara et al. performed two-row periodic wind farm simulations using an actuator disc approach combined with RANS. Comparisons with measurements showed that the numerical results indeed reached an acceptable level of accuracy in terms of velocity predictions and park performance. They also suggest that their study demonstrates that an appropriately designed wind farm arrangement can produce energy at levels similar to those of a sparse arrangement. Mikkelsen, Troldborg et al. performed wind turbine farm simulations with three turbines using the actuator line technique, where body forces are distributed along lines representing each blade. In the present study we follow up on earlier work by Ivanell et al., [5], where the influence of atmospheric turbulence was studied.

In the present work the wind field inside the Horns Rev wind farm 15 km outside the Danish west coast is simulated. The main emphasis is to determine the variation in production inside the farm as a function of turbulence intensity and wind direction. The simulation results are compared to measurements from the site. In the simulations a neutral boundary layer is used.

2 Numerical model

All simulations are performed using the EllipSys3D code developed at DTU/Risø. The EllipSys3D code is a general purpose 3D solver developed by N.N. Sørensen and Michelsen, [23], [13], [14]. The flow solver is based on a finite volume discretization of the Navier-Stokes equations in general curvilinear coordinates using multi-block topology using MPI. The code is formulated in primitive variables, i.e., pressure and velocity variables, in a collocated storage arrangement. Rhie/Chow interpolation is used to avoid odd/even pressure decoupling and the main solver is based

on multi-grid techniques. The pressure correction equation is based on the SIMPLE algorithm.

The numerical method uses a blend of third order QUICK (10%) and fourth order CDS (90%) difference schemes for the convective terms and a 2nd order central difference scheme for the remaining terms. This is a compromise between avoiding the non-physical numerical wiggles occurring when using forth order CDS and limiting numerical diffusion due to the upwinding nature of the QUICK method.

2.1 Actuator disc method

In the simulations we employ an extension of the Froude Actuator Disc (ACD) method. In this technique loading and actual geometry of the rotor blades are replaced by body forces that are distributed on an actuator disc. The forces are based on the local flow condition across the disc using tabulated aerofoil data and distributed in the computational domain in the direction normal to the disc.

An axis-symmetric actuator disc concept was developed, among others, by Sørensen and colleagues, [20], [19], [22]. A 3D approach was developed, among others, by Madsen, [8], [9]. The 3D method used here was implemented into the EllipSys3D code by Mikkelsen, [15].

The main idea with the actuator disc concept is to solve the flow past a rotor without resolving the boundary layer on the blades. With the ACD method, the number of node points at the blades is greatly reduced. Instead the focus is put on the resolution of the wake behind the turbines making the grid design easier and more efficient. The drawback, on the other hand, is that the method is based on tabulated aerofoil data, i.e. lift and drag coefficients, C_L and C_D, as a function of Reynolds number and angle of attack. As a consequence, the accuracy of the computed loading of the rotor depends on the quality of the applied data.

2.2 LES method

The computations are carried out as large eddy simulations (LES) employing the mixed sub-grid-scale model developed by Ta Phuoc, [24]. This model exploits the advantage of a closure combining vorticity and turbulent kinetic energy. In this model the vorticity is derived directly from the filtered variables whereas the turbulent kinetic energy is determined by use of a test-filter that is twice as coarse as the computational grid. For more details about the mixed scale model we refer to the text book by Sagaut, [18].

Using the coordinate directions (x_1, x_2, x_3), the Navier-Stokes equations are formulated as:

$$\frac{\partial u_i}{\partial t}+\frac{\partial u_i u_j}{\partial x_j}=-\frac{1}{\rho}\frac{\partial p}{\partial x_i}+f_{body,i}+f_{c,i}+\frac{\partial}{\partial x_j}\left[(\nu+\nu_t)\left(\frac{\partial u_i}{\partial x_j}+\frac{\partial u_j}{\partial x_i}\right)\right],\ \ \frac{\partial u_i}{\partial x_i}=0 \tag{1}$$

where u_i is the velocity vector, p is the pressure, t is time, ρ is the density of air, f_{body} represents the forces acting on the blades, f_c the corriolis force, ν is the kinematic viscosity and ν_t is the eddy viscosity that is modelled through the sub-grid-scale model.

When using the ACD method however, this viscosity parameter does not need to be exactly equal to the viscosity of air. Using the actual viscosity would leave us with a Reynolds

number, based on inflow velocity and rotor radius of several million, which would not be possible to compute on present day computer configurations. As a compromise between computer requirements and numerical resolution of the wake structures, the computations are carried out with an effective Reynolds number of 20,000, based on rotor radius and wind speed, on a mesh consisting of about 14 million mesh points. Since the flow we are considering is not wall-bounded it is not necessary to perform the simulations at the exact Reynolds number. Earlier computations, [21], [4], have demonstrated that the main dynamics are captured, provided that a certain minimum Reynolds number is utilized.

In order to avoid singular behaviour the body forces are smeared among neighbouring node points using a Gaussian distribution. The influence of that smearing parameter has been studied in a separate technical report, [4], and will therefore not be presented in detail here.

2.3 Wind shear

The averaged wind shear conditions that the turbines operates in are imposed at the inflow boundary. However, the numerical ability of flow solvers generally does not preserve the wind shear profile through the entire domain. In order to impose any wind shear profile, which may include directional change with height, the flow field is initially generated applying momentum sources everywhere in the domain, see Mikkelsen et al., [17]. The magnitude of the computed momentum sources is generally very small. In practice, an initial steady computation without the wind turbines included is performed in order to establish the force field required to obtain the desired mean wind shear profile. The resulting steady force field is stored and used in unsteady simulations with the wind turbines included. A power law wind shear profile with an exponent of α is chosen according to:

$$w(y) = \begin{cases} w_0 \cdot (c_2 y^2 + c_1 y) & y \leq \Delta \\ w_0 \cdot \left(\dfrac{y}{h_{hub}} \right)^{\alpha} & y > \Delta \end{cases} \tag{2}$$

where y is the height above the sea level, h_{hub} the hub height, w_0, c_1 and c_2 are parameters defining the profile from the sea level to a certain height Δ. α is set to 0.15 in the present simulations and defines the profile above Δ, which is set to 0.4 R.

2.4 Wind veer

The wind veer is defined as the change in wind direction as function of height. It has been shown that wind veer does exist in typical wind situations and in this study a wind veer distribution is added to identify to what extent wind veer affects the wake interaction. A wind veer of 2, 5 and 10 degrees across the disc area has been used in this study.

2.5 Aerofoil data

The actuator disc method uses tabulated aerofoil data taken from 2D measurements and modified for 3D and rotational effects. Data from the Tjaereborg and the Vestas V80 turbine have been used for all simulations in this project. The Tjaereborg rotor consists of NACA 4412-43 aerofoil sections and has a blade length of 29 m, giving a rotor diameter of 61 metres. The chord length was 0.9 m at the tip, increasing linearly to 3.3 m at hub radius 6 metres. The blades are twisted 1° per 3 metres. The tip speed was 70.7 m/s and the rotor solidity was 5.9 percent. The V80 blades have a

length of 39 m giving a rotor diameter of 80 metres. The Tjaereborg turbine is included into the analysis in order to compare results from different turbines. The turbines actually used at the Horns Rev are the Vestas V80, and the simulations with V80 should be used as basis for the measurement comparisons. The objective of the correlation is to distinguish how large an impact the blade data has on the wake interaction. In the present work all variables are made dimensionless such that the actual rotor configuration merely serves to produce a realistic load distribution. It should also be stated, that no active control of the turbines has been used in the simulations. At all times each turbine uses the tip speed ratio designed for a free stream velocity equal to the undisturbed wind speed. The V80 turbine in reality controls both tip speed ratio and blade pitch angles continuously.

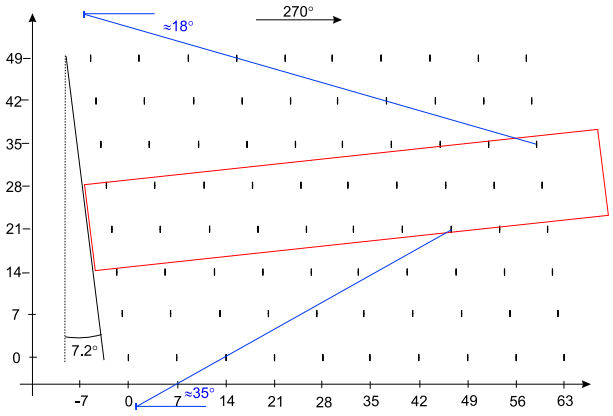

Figure 1: Layout of Horns Rev Wind Farm.

2.6 Atmospheric boundary layer

The influence of atmospheric turbulence is simulated by using a technique where turbulent fluctuations are imported in a 2D plane upstream the rotor from a pre-generated field which the flow solver then convects downstream toward the actuator discs. All pre-generated turbulent fields are generated by the Mann model, [11], [10], [12]. The simulations assume sea conditions defined by Charnock's relation, [2]. The turbulence intensity (u'/U) is set in the range of 2-5 percent. The use of the imposed atmospheric turbulence by introducing time-varying body forces in combination with the EllipSys3D code was recently implemented by Troldborg et al., [26].

The Mann model is based on the spectral tensor. The method models the spectral tensor (three-dimensional spectrum) using rapid distortion theory, implying a linearization of the Navier-Stokes equations, combined with an assumption of linear shear and a model for the eddy lifetime. The Mann model is capable of simulating all three velocity components of a three-dimensional incompressible turbulence field. The turbulent field is homogeneous, Gaussian, anisotropic and has the same second order statistics as the atmosphere.

The output is a spatial equidistantly spaced box where each downstream position corresponds to a timestep via Taylor´s frozen turbulence hypothesis.

When applying turbulent fluctuations from a pre-generated turbulent field, these are usually superimposed as velocity fluctuations to the mean velocities at the inlet. Troldborg et. al., [26], however, advocate a new approach where the turbulent field is introduced in a plane upstream the rotor, instead of introducing it at the inlet. Furthermore, instead of adding turbulent fluctuations directly to the mean flow, they propose to use unsteady concentrated body forces for generating the prescribed turbulent fluctuations. For numerical reasons, the loading at the plane upstream the rotor is smeared in a Gaussian manner. The body force can be expressed as:

$$\mathbf{f}' = \dot{m}\mathbf{u}'_m + \rho\epsilon\frac{\partial \mathbf{u}'_m}{\partial t} \qquad (3)$$

where $\dot{m}$ is the mass flow, ϵ a parameter that serves to adjust the smearing of the forces in a 1-D manner perpendicular to the plane and $\mathbf{u}_m$ is defined from the Mann turbulence box. This is done in similar manner as earlier described in the actuator line/actuator disc methods, [4]. In the present study ϵ is set equal to the size of a grid cell.

The Gaussian smearing is done by taking the convolution of the computed load $\mathbf{f}'$ and the regularization kernel η_ϵ.

$$\mathbf{f}'_\epsilon = \mathbf{f}' * \eta_\epsilon \qquad (4)$$

where $\mathbf{f}'_\epsilon$ is the loading in each point introducing atmospheric velocity variations and the regularization kernel is defined as:

$$\eta_\epsilon(z) = \frac{1}{\epsilon\pi^{1/2}}\mathrm{e}^{-(p/\epsilon)^2} \qquad (5)$$

where p is the normal distance between a grid point and the plane where turbulent fluctuations are imposed.

The resolution of the turbulence box is a factor 2 less than for the grid. Therefore both spatial and temporal interpolation is required to reach the velocity in each point and time.

2.7 Grid and boundary conditions

The main limitation of using the actuator disc method as compared to the previously used actuator line method, [4], [6], [7], is that individual tip vortices are not part of the flow. The size of the simulation does however require a simplification to be able to handle the number of turbines. By using the actuator disc method there is still need for further simplifications since a computation with all 80 turbines is beyond the available computational capacity. Therefore the two most central rows of turbines are simulated with periodic boundary conditions on the lateral boundaries. Accordingly, an infinitely wide farm is used. The Horns Rev wind farm contains 8 times 10 turbines. In the simulations, columns 4 and 5 are simulated with periodic conditions assuming an infinitely wide wind farm, see figure 1. This is a good approximation when the inflow angle is small compared to the direction of the rows. When the wind direction increases, contributions from non existing turbines outside the farm will be present. In this study we concentrate on wind directions in the range of plus/minus 15 degrees. Therefore the error from this approximation will be small since the "non-existing" turbines outside the farm are located approximately 18 degrees from the north boundary and 35 degrees from the south boundary to the turbines in the two centre lines that will be affected first, see figure 1. The inlet and the top surface are both set according to the wind shear profile discussed in section 2.3. The ground sur-

face is set with a wall condition. The outlet is set to convective conditions enabling vortices to cross. The mesh is designed by 52 blocks, allowing simulations to run on up to 52 processors simultaneously using MPI. Figure 2 shows the mesh design. There are 64 nodes on each block side, i.e., 64^3 nodes in each block giving a total number of nodes to $13.6 \cdot 10^6$.

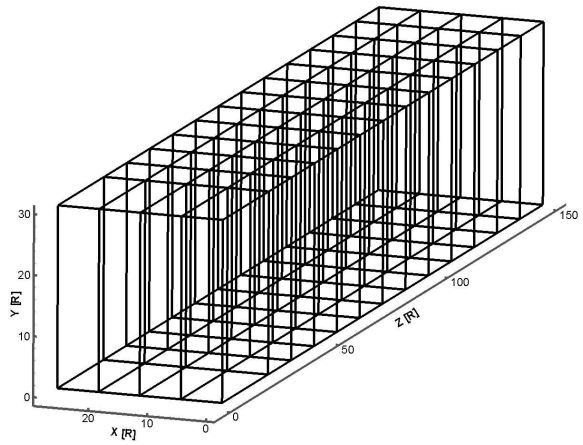

Figure 2: Block structure used for simulations of Horns Rev.

2.8 Time step and averaging

A typical time scale for the setup is in the order $\tau = 7D/U_\infty$, corresponding to the distance between the turbines.

Full development of wake interaction will occur at about $10\,\tau$ since there are 10 turbines in each row.

A turbulent box according to the definition in section 2.6 is generated. The size of the turbulence box is $28\text{R} \cdot 5\text{R} \cdot 224\text{R}$, where 28R corresponds to the width of the setup, 5R to the height of the turbulence box, where R is the rotor radius. The turbulence box, with a length of 224R, will pass one turbine in 896 physical seconds, s_{ph}, when the wind speed is 10 metres/second corresponding in time about 15 minutes.

$$\Delta z \approx \Delta x \approx \Delta = \frac{28\text{R}}{64 \cdot 4} = \frac{28R}{256} \approx 0.1\text{R} \tag{6}$$

where Δ corresponds to a typical mesh size. The polar grid representing the ACD consists of 21 nodes along the radius and 81 nodes during one revolution in azimuthal direction, i.e., about twice the resolution of the global grid. Δt is then set according to Δ. A numerical sensitivity study showed that:

$$\Delta t \approx \alpha \frac{\Delta x}{U} \tag{7}$$

where $U = 1$ in computational space gives result in the linear asymptotic independent range when α is set to 0.25.

2.9 Measurements

2.9.1 Turbulence intensity

The turbulence level at the site was measured before the erection of the wind farm. The measurements were made at a height of 62 m, [3]. The turbulence intensity is defined as:

$$TI \equiv \frac{u'}{U} \tag{8}$$

where u' is the rms value of the turbulent fluctuations and U is the mean velocity.

$$u' \equiv \sqrt{\frac{1}{3}(u'^2_x + u'^2_y + u'^2_z)} = \sqrt{\frac{2}{3}k} \tag{9}$$

$$U \equiv \sqrt{(U_x^2 + U_y^2 + U_z^2)} \tag{10}$$

where k is the turbulent energy.

Within the analysed sectors, 255-285 degrees, the turbulence intensity varies between 6.0% and 7.5% with a mean value of 6.9 percent. This value could be regarded as a high turbulence intensity when considering that there is open water in the westerly direction, which is the principal wind direction. When comparing these results with the Nysted wind farm on the east coast of Denmark, and its pricipally western winds over limited open water, there is significand difference in the turbulence of about 5%, [3]. The main reason for this is probably that the North Sea has greater wave heights compared to the site of the Nysted wind farm. Experience from these farms also shows that the turbulence intensity increases with increasing wind speed and wave height, [3]. The Charnock formula was used when simulating the turbulence field in the Horns Rev wind site, [2]. Therefore the turbulence intensity used in the simulations will be compensated for the effect of the wave height.

Figure 3 shows the result of the measurements at Horns Rev site before the erection of the wind farm. The result demonstrates that the turbulence level increases when the wind turns toward the south direction. The result also indicates that the turbulence intensity is higher for lower wind speeds. When analysing data for all wind speeds summarized from all wind directions (not shown in figure), it is evident that the turbulence intensity decreases up to 10 m/s, thereafter the turbulence intensity starts to increase linearly up to about 9 % at a wind speed of 26 metres/second, [3]. At 6 m/s and 8 m/s the mean turbulence intensity is about 8% and 6.8% respectively. Therefore, a windspeed of 10 m/s seems to result in the lowest turbulence intensity.

Using Charnock´s formula to generate the atmospheric turbulence, the turbulence intensity is reached according to the definition in section 2.9.1, equation 8, where the wind speed in this case only is used in the Mann model to create a realistic turbulent field using the Charnock formula with different wave heights. Therefore the wind speed set in the Mann model only serves as a parameter when setting the turbulence level.

$U_\infty[m/s]$	6.0	8.0	10.0
$TI[-]$	2.14	3.10	4.9

Table 1: Turbulence intensity related to free stream velocity.

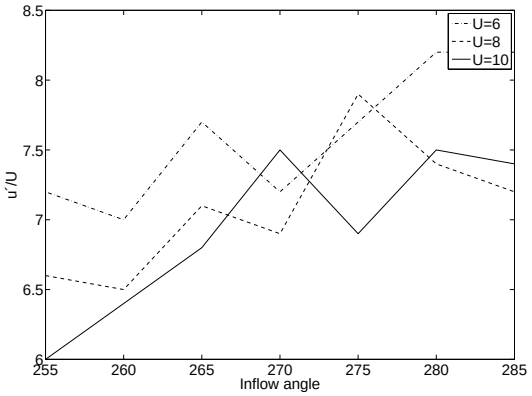

Figure 3: Measured turbulence intensity at Horns Rev wind farm at 62 m height. May 1999 to November 2002.

2.9.2 Production data

The production data were averaged for each wind sector between $255-285$ degrees and wind speeds from $6-10$ metres/second. The production data were averaged according to .

Each sector has been defined as the analysed inflow angle $\pm 2.5°$ and the wind speed to the analysed wind speed ± 0.5 metres/second. No filtering has been applied for the atmospheric stability and all data, taken in the period, May 1999 - November 2002, were included in the analysis. The following results show mean values of the fourth and fifth columns, both for measurement and simulations, except for figures 4 and 6 where results from columns four and five are separated.

Figure 4 shows the averaged production from the sectors with an inflow angle of 255 and 270 degrees. The result is only depicted for columns 4 and 5, i.e., the two most central columns in the farm. These two columns therefore correspond to an infinitely wide farm according to the discussion in section 2.7. The values have been normalized for the production of the first turbine. It is evident that the relative production decay in the farm does not depend on the wind speed. The 270 degree case corresponds to full wake interaction and the 255 degree case to the 15 degree inflow angle of the turbine column alignment. This corresponds to a case where wake interaction occurs at about the fourth turbine. In the figure, one can see that the local production decreases rapidly in the 270 degree case, while the production drop for the 255 degree inflow case occurs much further downstream. It is also apparent that, due to the higher turbulence intensity for the lower wind speeds, the wake interaction results in a lower production deficit.

Figure 5 illustrates the measured production at 10 ± 0.5 m/s for different

$U_\infty[m/s]$	*Sec.* 255[°]	*Sec.* 260[°]	...	*Sec.* 280[°]	*Sec.* 285[°]
$U_\infty = 6 \pm 0.5$	$255 \pm 2.5°$	$260 \pm 2.5°$	...	$280 \pm 2.5°$	$285 \pm 2.5°$
$U_\infty = 8 \pm 0.5$	$255 \pm 2.5°$	$260 \pm 2.5°$	...	$280 \pm 2.5°$	$285 \pm 2.5°$
$U_\infty = 10 \pm 0.5$	$255 \pm 2.5°$	$260 \pm 2.5°$	...	$280 \pm 2.5°$	$285 \pm 2.5°$

Table 2: Definition of sectors.

inflow angles. The black curves illustrate inflow of $\pm 15°$, the blue curves inflow angles of $\pm 10°$ and the red curves inflow angles of $\pm 5°$. The green curve shows the case with full wake interaction, i.e., zero degree inflow angle to the row alignment.

One can clearly see that for the cases with +(5, 10 and 15) degrees ('$\diamond$' in plot) inflow angle, the production is higher than for the cases with negative ('$*$' in plot) inflow angle. When comparing this with figure 3 one can reach the conclusion that a higher turbulence level will create more mixing between the wake and the ambient atmospheric flow, and thus provide a net transport of high-energetic flow to the turbines. There is also a geometrical aspect to the difference between the positive or negative inflow angles in relation to the row alignment. The turbines are located closer together when the wind direction is from south-west compared to a north-westerly wind due to the 7.2 degree tilt of the entire farm layout. The relationship between the size of these three different effects are however very difficult to distinguish.

Figure 6 shows the averaged data described in section 2.9.2 compared with a short time series where the conditions of the atmospheric boundary layer can be identified by the temperature variation with height. In the measurement series, the temperature is available at three different heights; one below the sea surface at -3 m, and two above the sea surface at 16 and 64 m height. The figures show 10 minute average values from two different times with a mean wind speed of 8 m/s and an inflow angle of 255 and 260 degrees. It is evident that there is a large variation between annular averaged values and shorter time series. Within the yearly averaged data, the boundary layer can be stable, non-stable or neutral to different extents depending on the different wind directions and velocities. When comparing simulation results with the yearly averaged data one must be careful about source validity of comparison values. No effort has been made to distinguish to what extent the boundary layer is neutral, stable or non-stable in the different wind sectors and wind speed intervals.

2.9.3 Wind veer

Measurement from the Horn Rev site has shown that wind veer exists and is in the order of 2-5 degrees across the disc, see figure 7. The figure illustrates wind veer probability as function of stability conditions, where s is stable, n neutral and u unstable. The results show the wind veer across half of the rotor disc, therefore, the wind veer across the entire rotor should be multiplied by a factor 2. The measurements indicate that during stable conditions, wind veer is most probably not present but large veer angles can occur. During unstable conditions there is a high probability that about 2-5 degrees of wind veer across the disc is present.

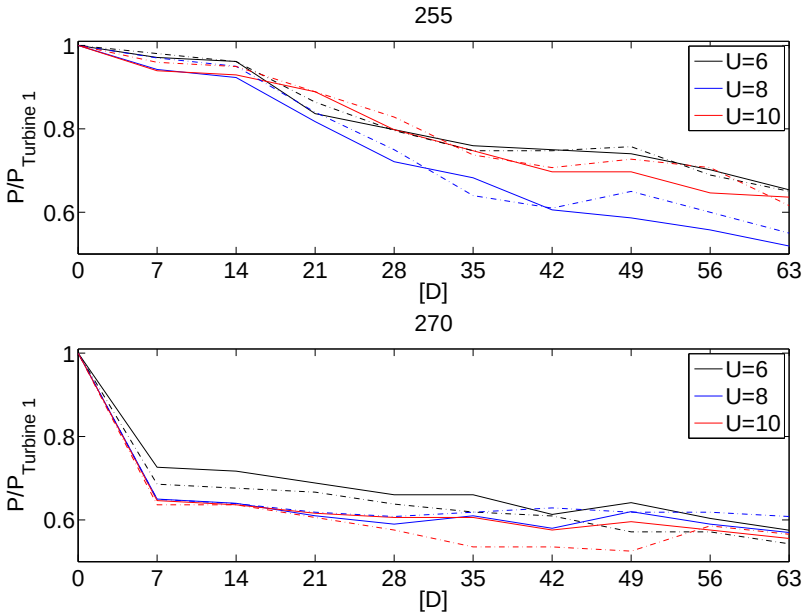

Figure 4: Experimental data from Horns Rev. The figures show the production at two inflow angles, 255 and 270 degrees. The solid lines represents the results for column number 4, and the dotted lines the results for column number 5. The result is depicted for three different wind speeds.

3 Results

3.1 Flow charactersitics

Figure 8 shows the flow at hub height for the three first turbines in column 5 at three different inflow angles, 265°, 270° and 285°, i.e., +5°, 0°, −15° to the column alignment. The wake interaction can be seen and it is obvious that the downstream turbines experience different flow features in the three cases depicted here.

One can clearly identify a stable vortex sheet from both the tip and root region of the disc. Note, however, that there is no distinct tip or root vortex since the actuator disc method is used. The sheet is clearly defined up to about one diameter downstream of the turbines in all cases in figure 8. In case (a) and (b) it is only present at the first turbine. In case (c) it is however seen at all turbines due to the large inflow angle.

3.2 Sensitivity

A sensitivity study is performed to identify the sensitivity of small changes of the inflow angle. This is especially interesting when analyzing the full wake case of an inflow angle of 270 degrees since the simulations with an inflow of that angle overestimates the deficit due to wake interaction when comparing with measurements. However, the measurements are based on a sector ±2.5°, that is a 267.5-272.5 degree inflow angle, whereas the simulation inflow angle is exactly 270° and therefore to a greater extent fulfills the full wake criteria.

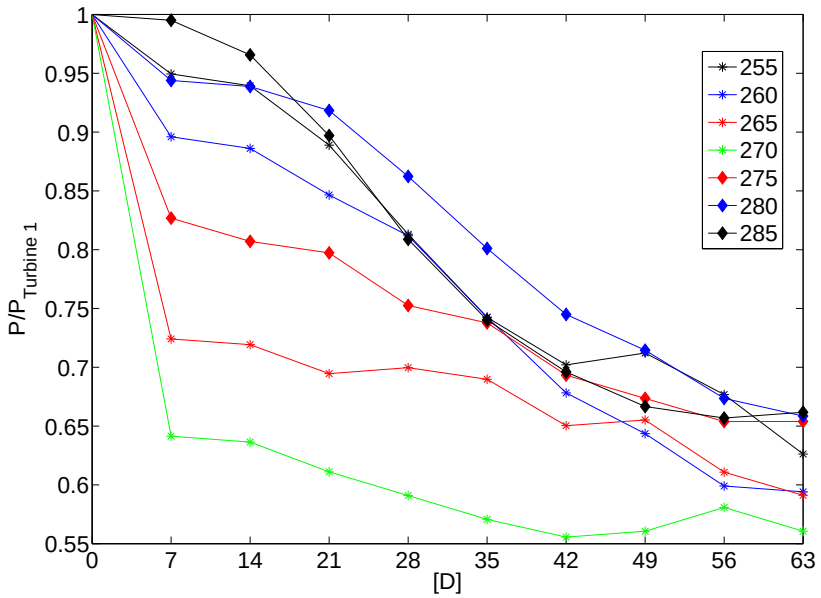

Figure 5: Experimental data from Horns Rev.

The result, see figure 9, shows that the production drop from the first to the second row decreases to a great extent when looking at inflow angles of 271-272 degrees.

3.3 Correlation with measurements

Figure 9 shows both measured and simulated results. The measured data are depicted in the same manner as in figure 5. The simulated results are plotted in the same colour as the measured data. The simulated cases with an inflow angle of -(5, 10 and 15) degrees are here plotted with a dotted line. Corresponding measured data are plotted with a '$*$'. The simulated cases with an inflow angle of +(5, 10 and 15) degrees are plotted with a solid line. Corresponding measured data are plotted with a '$\diamond$'. The case corresponding to full wake interaction, i.e., 270 degrees or 0 inflow angle to the column alignment, is here depicted with a solid green curve. The dotted and dashed curves correspond to inflow angles of +1 and +2 degrees, also discussed in section 3.2. All values have here been normalized with the production of the first turbine in the wind direction.

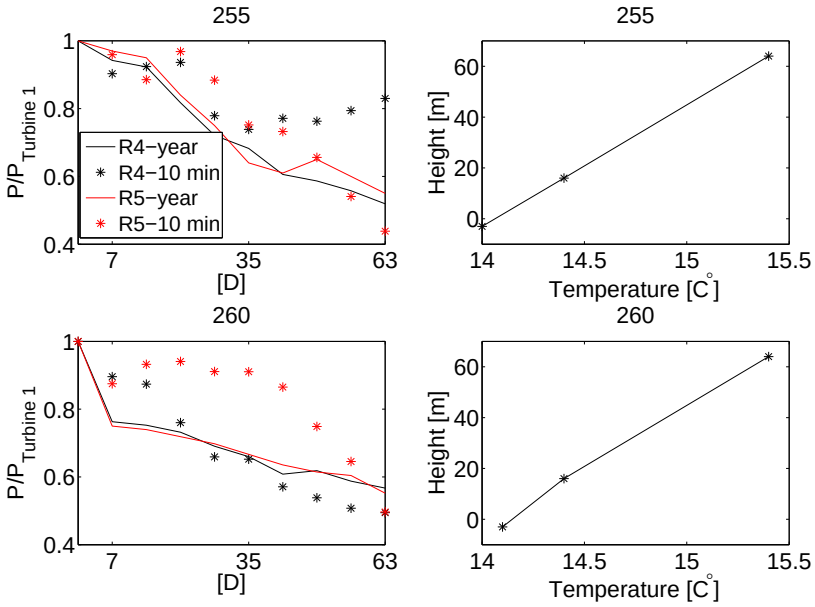

Figure 6: Experimental data from Horns Rev.

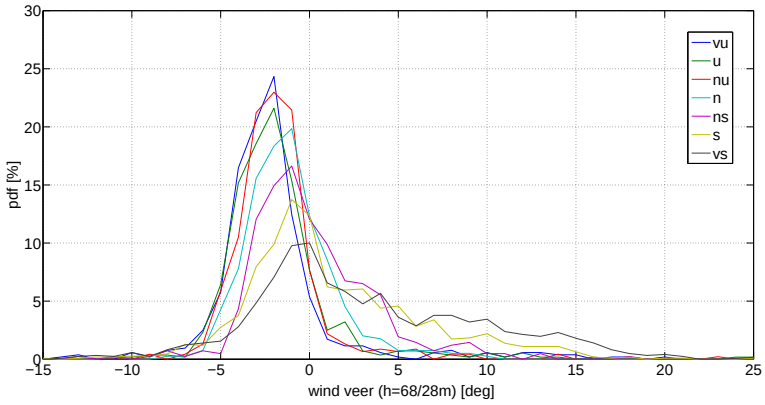

Figure 7: The figure shows the probability function of wind veer in Horns Rev. The data has been captured at 70 meters height in the time period 2003-2005. The data are captured from a wind direction from 0 to 210 degrees (according to the definition in figure 1) from a met mast outside the farm. (210-360 degrees has been left out because of interference from the wind farm.) Wind speeds between 5.5 and 10.5 m/s has been used.

Figure 10 shows the wake interaction of the different cases. Considering the case with an inflow angle of 285 degrees it is possible to identify

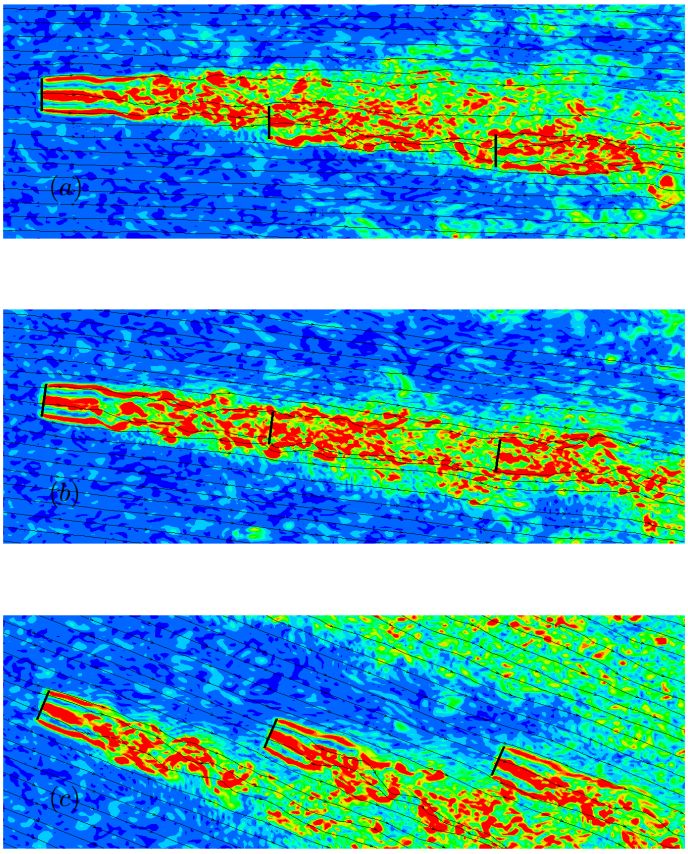

Figure 8: Vorticity at hub height. The figures illustrate different flow directions. The flow direction is identified by a number of stream-lines. (a) 265°, (b) 270°, (c) 285°.

how the wake interaction starts to be clearly noticeable at the fourth row of turbines. When comparing with figure 10, this corresponds to the position where the wake of the first turbine is getting close to a down-stream turbine. When looking further downstream, the production clearly drops essentially to the next row, i.e., the fifth row. When comparing with figure 10, this corresponds to where full wake interaction occurs. Further downstream the production levels out for about three turbines, after which the production again drops. The lowest production occurs at the ninth row, which corresponds to where the full wake interaction takes place for the second time.

When conducting the same analysis for the case with 280 degree of inflow angles, one can note similar behaviour. But now the essential drop of production occurs further downstream. When comparing with figure 10, one can observe that the wake from the first turbine passes the fifth turbine at a greater distance than the wake from the first turbine in the 285 degree case was to the fourth turbine. Therefore, the production drop for the fifth turbine is less than the drop for the fourth turbine in the 285 degree case. It is also obvious that the production for the sixth turbine, in the 280 degree case, is higher than the production of the fifth turbine in the 285 degree case. This is because in the 280 degree case, there is not a full wake interaction, compare with figure 10. When comparing these two cases with measurements the simulations underestimate the wake interaction until full wake interaction occurs and overestimate the wake interaction after the point of the first full wake interaction. However, it is important to remember that measurement data are based on a sector of $\pm$ 2.5 degrees while the simulations are performed at one exact wind direction.

When considering the cases with an inflow angle of $\pm$ 5 degrees, i.e., the 265 and 275 cases, it is noted that both results are between the measured data at rows one to four. When looking at figure 10 it is also evident that an inflow angle of $\pm$ 5 degrees could not affect the measured data to the extent as plotted in figure 9 where they deviate about 10 % compared to the production of the first turbine. Therefore one must conclude that the circumstances of the measuring peroid for the cases with $\pm$ 5 degrees inflow angle are different due to reasons earlier discussed in section 2.9. The simulated results are however in the same order as the measured data which should verify that the levels of the simulated production are well predicted. Further downstream the case with -5 degree of inflow angle results in slghtly higher values compared to the case with an inflow angle of +5 degrees. That could be explained by the geometry of the farm. The cases with north inflow angles experience a longer distance to the next turbine of the south column compared to a case where the wind is coming from the south, and the distance to the next turbine in the north column is shorter. Full wake interaction would occur at about the eleventh row, however this case has only 10 rows so the effect will be small. The last drop in the -5 degree case, i.e., between the ninth and tenth row, may however be influenced by the wake from the first turbine.

When considering the full wake case, i.e., the 270 degree case where full wake interaction occurs since the wake from the upstream turbine fully hits the downstream turbine, it is clear that the simulation overestimates the wake interaction. However, when considering that the measured data are based on a sector of $\pm$ 2.5 degrees and comparing also with a simulation using inflow angles of +1 and +2 degrees, the overestimation does not appear to be

as large as first predicted.

The variation of the measurement data are in some cases caused by variation of measurement conditions with inflow angle. The linear wake model correlates well with the simulation results. It is, however, important to remember that the simulations are based on a simplified model performed with one exact wind direction and one boundary layer profile. In reality the boundary layer profile, as has been shown, will vary in time depending on temperature but also most probably on wind direction. The wind direction used here is also a 10 minutes average value that does not quantify the distribution of the wind direction change. Therefore, the non correlating data might be explained by this. For example, in the $\pm$ 10 degrees cases where the measurements show a large deficit at the position of the second turbine while the simulations show no deficit, a change in wind direction could result in wake interaction at the second turbine.

Figure 11 shows the influence of wind veer. When adding two degrees of wind veer across the rotor disc, the full wake interaction agree very well with measurements. When adding five degrees of wind weer, to the full wake case, the simulation underestimates the wake interaction compared to measurements. When considering the 275 degree case, the simulations without wind veer agree better with measurement. In this case the production is also decreased compared to the simulation without wind veer. That differ from the full wake case, where the production instead is increased. Generally one should expect a reduction in production since the wind veer decreases the wind speed orthogonal to the rotor disc. However, when wake interaction occurs, the wind veer might decrease the wake interaction effect and therefore increase the production. The results indicates realistic results. However, this complicated flow situation is highly dependent of parameters in the measurements, such as stability wind direction distribution etc.

The results in figure 11 clearly indicates that wind veer has a significant impact on the flow inside the wind farm. When considering the case with 2 degrees wind veer across the disc area, simulations of the full wake interaction case (270 degrees) corresponds to measured results to a great extent. This, therefore, illustrates that when also considering wind veer in the simulation, very complicated flow situations can be described by this method.

4 Conclusions

Large eddy simulations of the Navier-Stokes equations are performed to simulate the Horns Rev off shore wind farm, which is situated 15 km outside the Danish west coast. The aim is to achieve a better understanding of the wake interaction inside the farm. The simulations are performed by combining the in-house developed computer code EllipSys3D with the actuator-disc methodology.

In the present study approximately 13.6 million mesh points are used to resolve the wake structure in the park that contains 80 turbines. The two central columns of turbines have been simulated with periodic boundary conditions. This corresponds to simulating an infinitely wide farm with 10 turbines in a downstream direction. Simulations have been performed within

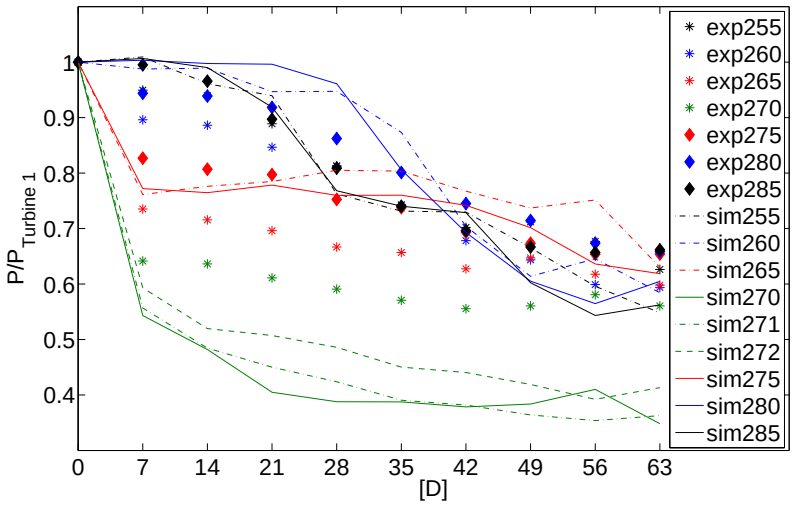

Figure 9: Simulation results compared with measurements. Results from both simulations and measurements are shown for inflow angles between 255 and 285 degrees, i.e., ± 15 degrees from the westerly direction.

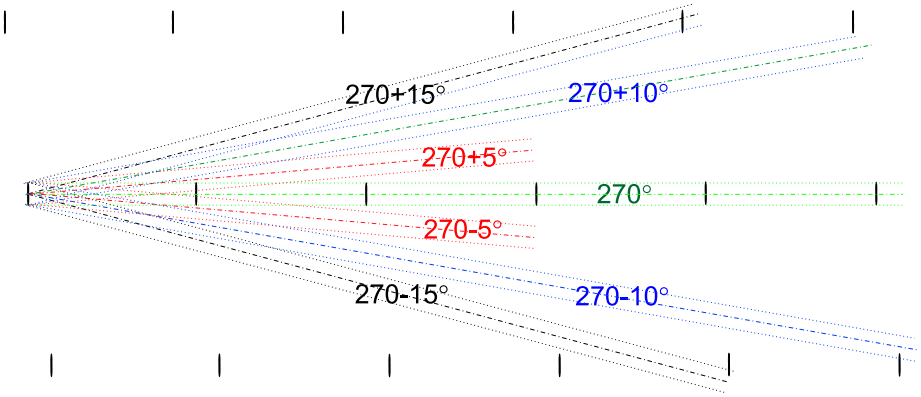

Figure 10: Wake interaction model of the linear extent of the wake due to different wind directions.

plus/minus 15 degrees of the turbine alignment.

The study shows that the method used captures the main production variation within the wind farm. The result further demonstrates that levels of production correlate well with measurements.

Seen in the light of the big uncertainties, the computations showed very good correlation with the measurements.

The study also shows that the wind veer has a significant impact on the wake interaction.

Future work will especially concentrate on wind veer.

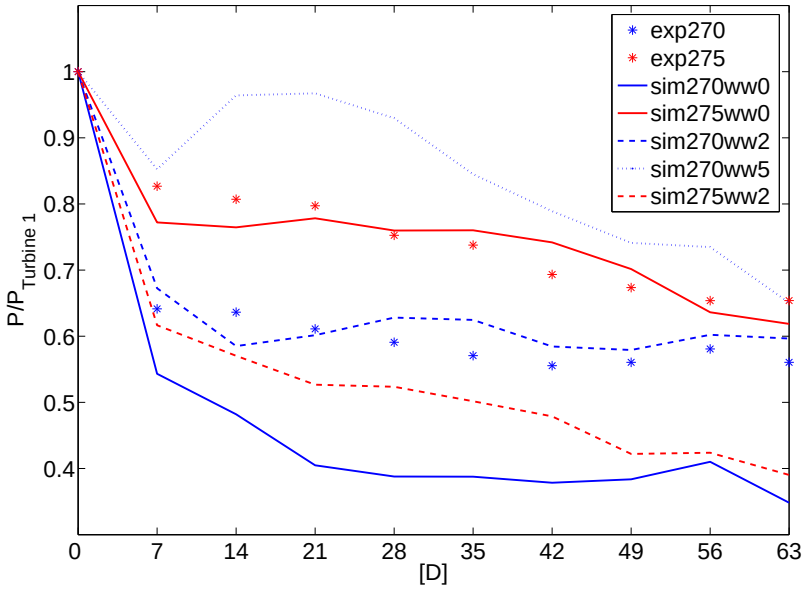

Figure 11: Simulation results compared with measurements. Results from both simulations and measurements are shown for inflow angles between 270 and 275 degrees. Results without wind veer are compared with results including wind veer.

5 Acknowledgments

Vattenfall and DONG Energy are acknowledged for providing measurement data from Horns Rev and Vestas for providing aerofoil data from the V80 machine.

References

[1] I. Ammara, C. Leclerc, and C. Masson. A vicous three-dimentional differential/actuator-disc method for the aerodynamic analysis of wind farms. *Journal of Solar Energy Engineering*, 124:345–356, 2002.

[2] H. Charnock. Wind stress on water surface. *Q.J.R. Meteorol. Soc.*, 81:639–640, 1955.

[3] K. S. Hansen. In private communication he showed unreported data put together from measurements of horns rev wind farm. the data originated from dong energy and was put together within the upwind project. Technical report, DTU, 2008.

[4] S. Ivanell, R. Mikkelsen, J. N. Sørensen, and D. Henningson. Validation of methods using ellipsys3d. Technical Report Trita-mek 2008:12, 2008.

[5] S. Ivanell, R. Mikkelsen, J.N. Sørensen, and D. Henningson. Three-dimensional actuator disc modelling of wind farm wake interaction. In *Proceedings of the European Wind Energy Conference and Exhibition*, number PO.149., Brussels, 2008.

[6] S. Ivanell, R. Mikkelsen, J.N. Sørensen, and D. Henningson. Stability analysis of the tip vortices of a wind turbine. *Wind Energy: Accepted*, 2009.

[7] S. Ivanell, J.N. Sørensen, R. Mikkelsen, and D. Henningson. Analysis of numerically generated wake structures. *Wind Energy*, 12(1):63–80, 2009.

[8] H. A. Madsen. A cfd analysis of the actuator disc flow compared with momentum theory results. In *IEA Joint Action - Aerodynamics of Wind Turbines, 10th Symposium, Edinburgh*, 1996.

[9] H. A. Madsen. Yaw simulation using a 3d actuator disc model coupled to the aeroelastic code hawc. In *IEA Joint Action - Aerodynamics of Wind Turbines, 13th Symposium, Stockholm*, 1999.

[10] J. Mann. The spatial structure of neutral atmospheric surface-layer turbulence. *Journal of Fluid Mechanics*, 273:141–168, 1994.

[11] J. Mann. Wind field simulation. *Prob. Engng. Mech*, 13(4):269–282, 1998.

[12] J. Mann, S. Ott, B. Hoffmann Jørgensen, and H. P. Frank. Wasp engineering 2000. Technical Report Risø-R-1356(EN), 2002.

[13] J. A. Michelsen. Basis3d - a platform for development of multiblock pde solvers. Technical Report AFM 92-06, Dept. of Fluid Mechanics, Technical University of Denmark, DTU, 1992.

[14] J. A. Michelsen. Block structured multigrid solution of 2d and 3d elliptic pde's. Technical Report AFM 94-06, Dept. of Fluid Mechanics, Technical University of Denmark, DTU, 1994.

[15] R. Mikkelsen. *Actuator Disc Methods Applied to Wind Turbines*. PhD thesis, Dept. of Fluid Mechanics, Technical University of Denmark, DTU, 2003.

[16] R. Mikkelsen, J. N. Sørensen, S. Øye, and N. Troldborg. Analysis of power enhancement for a row of wind turbines using the actuator line technique. *Journal of physics: Conference series, The science of making torque from wind*, 75(012044), 2007.

[17] R. Mikkelsen, J. N. Sørensen, and N. Troldborg. Prescribed wind shear modelling with the actuator line technique. In *Proc. of EWEC 2007, European Wind Energy Conference*, Milano, 2007.

[18] P. Sagaut. *Large Eddy Simulation for Incompressible Flow*. Springer, 3 edition, 2006.

[19] J. N. Sørensen and C. W. Kock. A model for unsteady rotor aerdynamics. *Journal of Wind Energy and Industry Aerodynamic*, 58:259–275, 1995.

[20] J. N. Sørensen and A. Myken. Unsteady actuator disc model for horizontal axis wind turbine. *Journal of Wind Engineering and Industry Aerodynamics*, 39, 1992.

[21] J. N. Sørensen and W. Z. Shen. Numerical modeling of wind turbine wakes. *Journal of Fluid Engineering*, 124, 2002.

[22] J. N. Sørensen, W. Z. Shen, and X. Munduate. Analysis of wake states by a full-field actuator disc model. *Wind Energy*, 1:73–88, 1998.

[23] N. N. Sørensen. *General perpose flow solver applied to flow over hills*. PhD thesis, Risø National Laboratory, Roskilde, 1995.

[24] L. Ta Phuoc. Modeles de sous maille appliques aux ecoulements instationnaires decolles. In *Proc. of the DRET conference: 'Aerodynamique Instationnaire Turbulents - Aspects Numeriques et Experimentaux*, 1994.

[25] N. Troldborg. *Actuator Line Modeling of Wind Turbine Wakes*. PhD thesis, Dept. of Fluid Mechanics, Technical University of Denmark, DTU, 2008.

[26] N. Troldborg, J.N. Sørensen, and R. Mikkelsen. Actuator line simulation of wake of wind turbine operating in turbulent inflow. *Journal of physics: Conference series, The science of making torque from wind*, 75(012063), 2007.